Using blind-tests for database evaluation in the prediction of rotational-translational landslides in the Tirano North area, northern Italy

A. G. Fabbri[1], M. R. Mauriello[1] & C. J. Chung[2]
[1]*DISAT, Università di Milano-Bicocca, Milan, Italy*
[2]*SpatialModels Inc., Ottawa, Canada*

Abstract

This contribution deals with the integration of spatial data to predict landslide hazard. A database is used containing the spatial distribution of landslides that have occurred in a study area in the northern part of the "Comunità Montana Valtellina di Tirano", in the Lombardy Region of northern Italy. The mountain area is affected by a large number of rotational-translational landslides. The database consists of digital maps of both continuous and categorical data that are considered as influential in determining the conditions of sliding and is to allow the identification of spatial relationships between the distribution of observed-mapped landslide trigger zones and that of the integrated map units of the more-or-less "influential" digital maps. Functions of those relationships are used for the characterization and recognition of either known trigger zones or future ones, over the entire study area.

Given a mathematical model to establish the spatial relationships using a database, their integration within a study area to generate a landslide hazard map, must be tested for relative significance and quality for the purpose of hazard prediction. For this the dedicated software system Spatial Target Mapping, STM, is used that provides iterative blind testing procedures for a number of spatial prediction models. The analyses, based on empirical likelihood ratios and many blind tests, have clearly identified the capabilities of the database in its present condition for prediction modelling of landslide hazard.
Keywords: landslide hazard, spatial relationships, data integration, likelihood ratios, spatial prediction, blind tests, database evaluation.


WIT Transactions on Information and Communication Technologies, Vol 44, © 2012 WIT Press
www.witpress.com, ISSN 1743-3517 (on-line)
doi:10.2495/RISK120231

1 Introduction and motivation

Numerical approaches to assess or predict natural hazards stem from the efforts to establish spatial relationships between the occurrence of hazardous events and their spatial context. This became possible with the availability of systematic descriptions and interpretations of hazardous events, such as specific dynamic types of landslides, including their distribution in space and in time over a study area. Their geomorphologic settings could be identified by considering the distribution over the study area of units in thematic maps related with the hazard generating processes: characteristics of the topographic surface, elevation, slope, aspects, etc., and of land-use, vegetation, soil depth, surficial and bedrock geology. The numerical approaches were applied to spatial databases containing those distributions of hazardous occurrences and of characteristic map units. Within the databases aspects such as location and extension of trigger zones (scarps) and the entire landslide bodies (scars), dynamic type and time of occurrence needed to be recorded with a convenient level of spatial resolution, hopefully compatible with that of the thematic units. The units represented either continuous fields (e.g., slope) or categories (e.g., classes of land use).

In most studies and applications to date, much emphasis has been assigned to the construction of the mathematical models and to assessing their superiority over alternative models in terms of their success in classifying the level of hazard over the study areas [1]. Less attention was given to interpreting the resulting hazard maps. Such studies were criticized by the authors of this contribution because of the absence of validation measure of the hazard maps generated by modelling [2]. Various types of cross-validation were proposed, in which blind-tests were strategically applied to assess the relative quality, robustness, uncertainty or comparability of the hazard maps. Those tests were based on modifications of the inputs to the models, for instance ignoring part of the occurrences or of the study area, or changing assumptions on the data.

In this contribution blind-tests are used as a strategy to bring out database suitability for prediction modelling of landslide hazard. A database is used containing the distribution of landslide events that have occurred in a study area in northern Italy, which is affected by a large number of trigger zones of rotational-translational landslides. This paper deals with the database, its suitability for the modelling of the spatial relationships, the processing strategies used, and the analyses performed using the Spatial Target Mapping system, STM, especially developed for prediction modelling with iterative spatial cross-validation procedures.

2 Database construction and use

The study area, whose location is shown in Figure 1, covers the northern half of the "Comunità Montana Valtellina di Tirano", in the Province of Sondrio, Lombardy Region of northern Italy.

The "Comunità" has been established in 1971 for the protection of mountain communities. It consists of 12 municipalities covering altogether 450 km^2. An

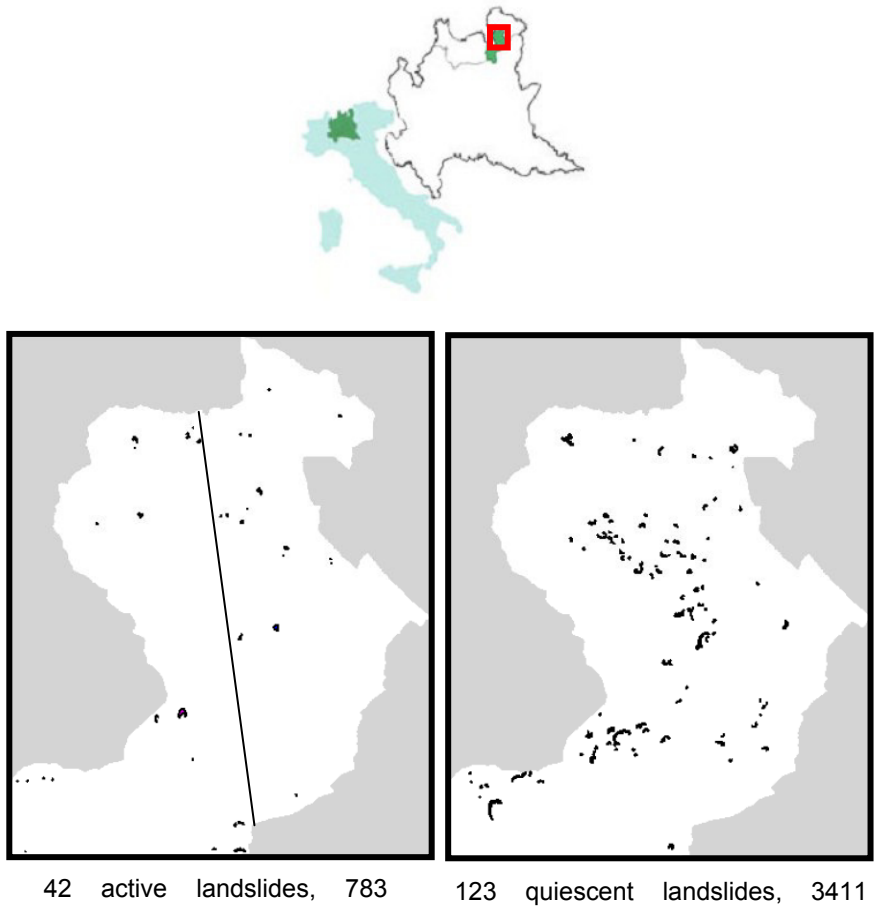

Figure 1: Location of the Tirano North study area, Lombardy Region, above, and distribution of active and quiescent rotational-translational landslides, below. The line separates the study area in W and E regions.

overview of its geomorphology was provided by Mauriello [3] and is summarized here. Over 67% of the territory has elevations higher than 1500 m a. s. l. The valley bottoms, traced by the Adda River, have a number of connected planar areas flanked by alluvial fans. The area has a young Alpine geomorphology due to the morphogenic action of waters and glaciers. Erosion, due to torrent action is predominant: the intense activity of the waters generates erosion of both sides of stream beds, triggers landslides and mass movements in areas affected by deep gravitational deformations or paleo-landslides. In addition, the exploitation of the waters for electrical energy production has generated slope instabilities due to the induced variations of aquifer conditions.

The area is characterized by Alpine tectonism with different structural domains and intensities of deformation. It is crossed by a linear tectonic structure representing an over-thrust surface and is marked by mylonites representing an advanced state of deformation. The land use is mostly related to climatic conditions and varied geomorphology with elevations ranging between 300 m and 4000 m a. s. l. that affect temperature, pressure, rainfall, humidity and insolation. Rainfall has yearly averages between 1300 and 1900 mm, in areas of greater precipitations, and between 700 and 900 mm, in areas of minor precipitations. The rainfall variations occur mostly in spring and in summer. The vegetation distribution is strongly influenced by elevation differences: up to 600-700 m a. s. l. are broad-leafed woods, at higher elevations up to 1400 m and sporadically to 2300 m are coniferous woods. At the valley bottoms and on less steep surfaces, anthropization has greatly affected the vegetation with clear cutting of woods for agriculture purposes, or the construction of terraces for vineyards and orchards. Urbanization that used to be located mostly on natural terraces, well protected from floods and slope failures, has expanded with the occupation of the valley bottoms and of the alluvial fans where now most of the villages are now distributed.

The most frequent dynamic types of mass movements in the study area are *rotational* and *translational slides* that affect debris slope deposits, accumulations of paleo-slides or fluvio-glacial deposits. Triggering cause is the convergence of several factors such as intense rainfall and stream erosion at the valley bottoms. Rotational slides or slumps occur in terrains and poorly-coherent or semi-coherent rocks, poorly cemented, altered or brecciated by tectonism. Flows, rock avalanches, debris flows and debris torrents are impossible to separate in the study area. Complex slides due to convergence of several dynamic types are predominant. The transport phase of the material is relatively reduced and the erosion area or detachment niche can be separated from the accumulation area not too far down the slope. The depletion zone can be distinguished from the accumulation zone. The mobilized material is divided into main body and toe of the landslide.

The Tirano North study area database [3] covers a rectangular area with 1034 pixels x 1290 lines, with pixels of 20m resolution. Within the rectangle, the study area occupies 742,624 pixels, i.e., 297 km^2. Beside a field trip volume dedicated to Alpine Landslides in the area [4], three national-regional initiatives provided fully or in part the data for the construction of the spatial database: projects IFFI [5], on landslide inventory, CARG [6] on geological cartography, and DUSAF [7], on soil-land use cartography. Such a wealth of controlled information allowed the construction of a database with a relatively high quality of information.

In the database a distinction could be made of the activity status of the landslide phenomena into active and quiescent. Active were considered the landslides directly observed as in-motion or with a seasonal recurrence cycle characteristic of their evolutionary process. Quiescent were considered those non active at the time of surveying and lacking a seasonal periodicity. For these, ample data were available demonstrating past activity within the

geomorphologic, morpho-climatic and morpho-dynamic system in the region. Conclusion is that they retain a possibility of reactivation, not having exhausted their evolution potential.

There are 42 active landslides trigger zones in the area that occupy 783 pixels (average size 18.64), and 123 quiescent landslide trigger zones that occupy 3411 pixels (average size 27.73). Figure 1 shows the location of the Tirano North study area and the distributions of the 42 active and 123 quiescent rotational-translational landslides. The total trigger zones of 4194 pixels, represents 0.56% of study area. It was not possible to separate rotational from translational landslides either in the field or from the inventories consulted. For this reason the study dealt with rotational-translational landslides. Table 1 provides some numerical information on the spatial database of the Tirano North study area. For it was available 1:10,000 digital cartographic information. The digital terrain model had a 5 m resolution that was used to obtain the 20m resolution derived digital maps of the database.

Table 1: Data layers, support, value ranges and data type of the Tirano North study area database [3]. Supporting patterns are defined in section 3.

Data layer	Supporting pattern	Value range	Data type	Data source
Quiescent landslides	Direct	1 - 123	Sequentially indexed	IFFI [5]
Active landslides		1 - 42		
land use	Indirect	1 - 20	Categorical	DUSAF [7]
lithology		1 - 44		CARG [6]
permeability		1 - 8		
elevation		389 - 3313	Continuous	Aerial photo-grammetric survey of year 2001: 1:2,000-1:10,000
slope		0 - 77		
aspect		0 - 359		
Internal relief		1 - 157		
curvature		-41 - +39		

3 Modelling spatial relationships using STM

The database described in the previous section was processed and analyzed using the Spatial Target Mapping system, STM, [8] a software tool for the application of a variety of prediction models, whose resulting prediction maps are conveniently subjected to cross-validation procedures for interpretation [9, 10]. STM is a development of an earlier system, the Spatial Prediction Modelling system, SPM [11]. The models are based on functions such as Fuzzy Sets, Empirical Likelihood Ratios, Linear and Logistic Regression, and Bayesian Probability. The functions can be used as alternative interpretation and ways to transform each data layer into a supporting pattern of the presence and absence

of the occurrence of hazardous events. A proposition is implied in the form of a mathematical statement to be proven as true or false: i.e., "that a pixel in the study area is affected by the trigger zone of a rotational-translational landslide." The combined presence of the mapping units of the data layers is used to express the support of the proposition.

The function is estimated from the database of the study area and is calculated for every pixel in it as a relative hazard value. The set of the pixels and their values so calculated represents the hazard prediction will. The simultaneous analysis of continuous and categorical data layers includes their aggregation into a favourability index function of landslide hazard.

The data layer with the distribution of the trigger zones of the landslides is considered as a *direct supporting pattern*, DSP, while those of the other data layers are termed as *indirect supporting patterns*, ISP. In this work we have used the Empirical Likelihood Ratio function, ELR, as a model to generate and cross-validate landslide hazard prediction maps. We will term them *prediction patterns* from now on. A full discussion of this model has been provided in by Chung [12].

For a given study area, the degree of completeness of a spatial database is a consequence of time, means and urgency of the hazard study. However, the quality of the resulting hazard prediction pattern, expressing the likelihood of future occurrences, depends on several factors of both conceptual and empirical nature. Assumptions are necessary on the uniformity of rate of occurrence through time and space, on that of the triggering factors, on the capability of the database to provide reliable spatial relationships, and on the mathematical models used to extract, classify and extrapolate the typical geomorphologic setting of the hazard. Such setting is obtained by aggregating the spatial relationships established by the models for each thematic map.

In the application of the ELR to the database, the following assumptions are necessary or implicit:

(1) The database is sufficient in area extent, resolution and content to express the spatial-temporal characteristics of the hazardous process;
(2) The ISPs represent factors of, or indicators related to, the presence of the hazardous events; therefore they sufficiently express the spatiality of the process generating the distribution of the hazardous events;
(3) The DSP can be partitioned to represent older and younger sets of occurrences, so that the older set is used to compute the spatial relationships to generate classes of hazard, and the younger set is used to verify the distribution of younger occurrences among the higher classes of hazard;
(4) The conditions in space and in time of the older set are similar and comparable to those of the younger set;

In this study DSPs are obtained from the map with the distribution of all the 165 rotational-translational landslides, and from various partitions of that distribution, e.g., that of the 123 quiescent landslides, that of the 42 active landslides and further sub-partitions of those. In addition, the ISPs are obtained from transforming the five continuous data layers (elevation, aspect, slope,

internal relief, and curvature) and the three categorical data layers (lithology, land use and permeability). The transformation is based on computing the density function for the continuous data layers in correspondence with the DSP (or the normalized frequency for the categorical data layers), and the density function in correspondence with the areas outside the DSP. Then the ratio of the two is calculated for each value or unit of a data layer.

The ELR function model was applied initially to the database using the distribution of all the 165 landslides and subsequently using separately those of the active and quiescent landslides. In the analyses performed all eight ISPs were used and integrated to generate relative ranks of the ELR values. Figure 2 shows two predicted hazard prediction patterns in which groups of classes in descending order are assigned a sequence of pseudo-colours as indicated by the legend. From an initial default number of 200 equal area classes, each of 0.5% of the study area, classes were aggregated for facilitating the visualization of the pattern. In the illustration, in white are the landslides used for generating the hazard prediction patterns and in black the remaining landslides that we would like to see as well classified, i.e., assigned to a high value hazard class. In either

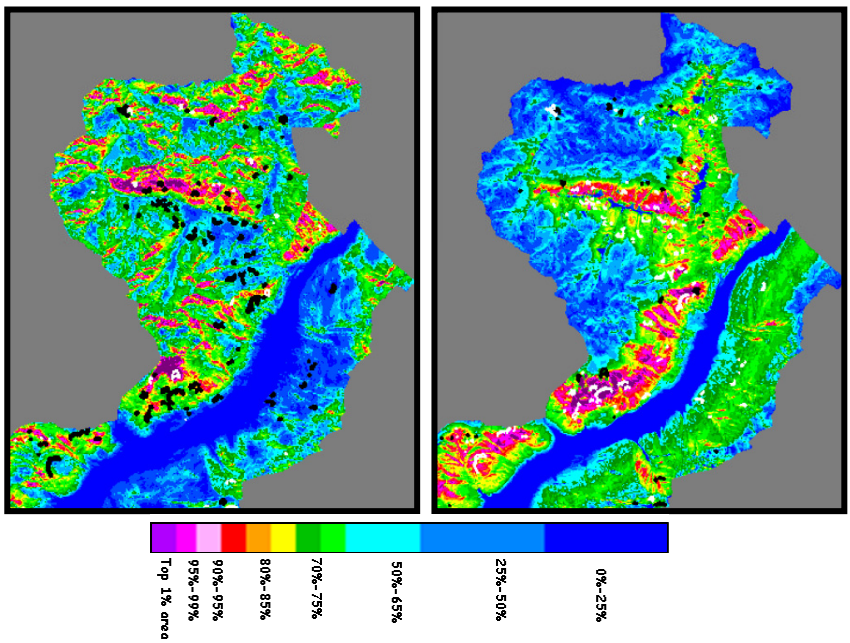

Figure 2: Prediction patterns, left, using 42 active landslides in white and, right, using 123 quiescent landslides in white. In black is the distribution (size slightly exaggerated for better visualization) of the remaining 123 quiescent landslides, left, and of the 42 active landslides, right. Legend indicates the hazard classes as % of study area; grey is the outside of the study area.

pattern we can see that a high proportion of the black landslides are located on low-value classes. Figure 3 shows the fitting-rate curves and the prediction-rate curves for the two prediction patterns in Figure 2. The cumulative curves are obtained as follows. The study area ranked equal-area classes are on the horizontal axis in descending order, and on the vertical axis are the corresponding cumulative proportions of landslides. The fitting-rate curves express the distribution of the landslides used for generating the prediction pattern and do not indicate the prediction quality but only the classification fit. The prediction-rate curves instead, indicate how well the cross-validation landslides (i.e., not used to predict) are distributed among the prediction classes. They are the key for representing the relative quality or "goodness" of the hazard prediction classes. For instance, comparing the two prediction-rate curves at 10% and 20% of the highest hazard classes in the study area, we have a corresponding 10% and 30% of quiescent landslides in the prediction using the 42 active landslides, and 18% and 28% of active landslides in the prediction using the 123 quiescent landslides. The two prediction-rate curves show a very poor prediction power! Let us see what the cause is.

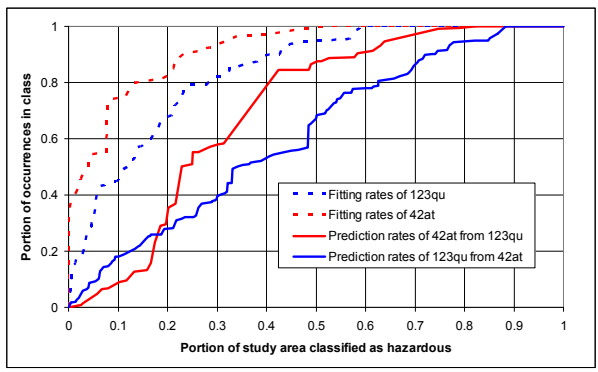

Figure 3: Fitting-rate curves (broken lines) and prediction-rate curves (solid lines) for the two prediction patterns in Figure 2, obtained using the distribution of the 42 active landslides and the 123 quiescent landslides, respectively.

The poor predictions in Figure 2 reflect the situation in which the two groups of active and quiescent landslides have different distributions and settings. Initially it was hoped that the quiescent landslides were just older than the active ones or that a prediction using the active ones would indicate the quiescent landslides that are likely to reactivate. In this case we have a different interpretation.

The different settings can be confirmed and interpreted by analyzing the support of the individual ISPs, observing their density functions and ELR functions. For instance, in Figure 4 we observe the density function of elevation for the entire set of 165 landslides and their outside, and the corresponding ELR function. Values of ELR above 2 indicate acceptably significant ratios. The

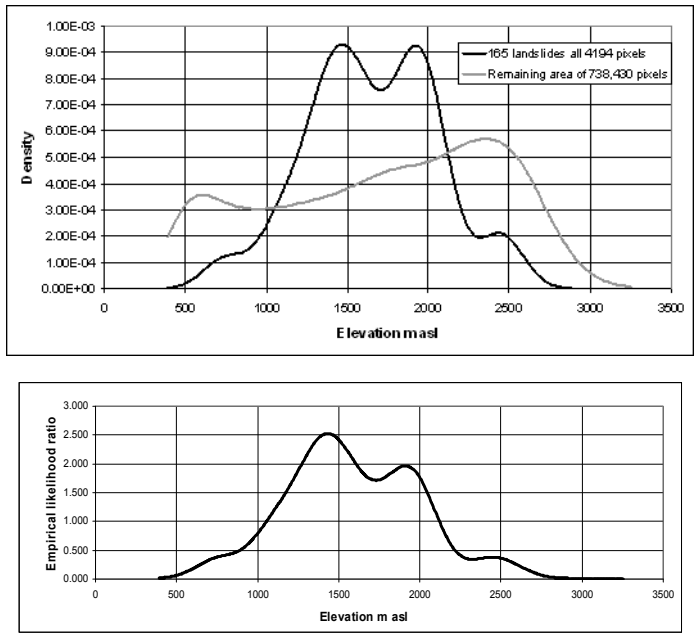

Function

Figure 4: Density function and Empirical Likelihood Ratio function of the elevation data layer for the entire set of 165 landslide trigger zones (4194 pixels), without distinction of activity status, contrasted with the remaining area (738,430 pixels), in the Tirano North study area.

bimodality shown in both the density function in correspondence with the 165 landslides and in the ELR function already indicates the existence of two maxima at about 1400 m and 1900 m elevations.

Figure 5 shows the ELR functions of elevation and slope separately for the two landslide activity sets. Elevations of about 1400 m are common for the distribution of quiescent landslides, and around 2000 m for active landslides.

Slope angles between 40 and 50 degrees have significant ELR values for active landslides but it is not so for quiescent landslides. Also internal relief values greater than 70 and aspect values between 42 and 112 generate ratios well above 2. On the contrary, the curvature ratios, land use and permeability do not show much significance of support.

Figure 6 shows the normalized frequency function, and the ELR functions of lithologies for the 42 active landslides. Of the 44 lithologies, glacial drift, non colonized or poorly colonized rock debris accumulations (units 15, 16), eluvial-colluvial deposits, exposed intrusive rocks (units 37, 38, 39), and generally incoherent debris (unit 21) have significant frequencies and high ELR values as well for active landslides. Quiescent landslides, their diagram is not shown here,

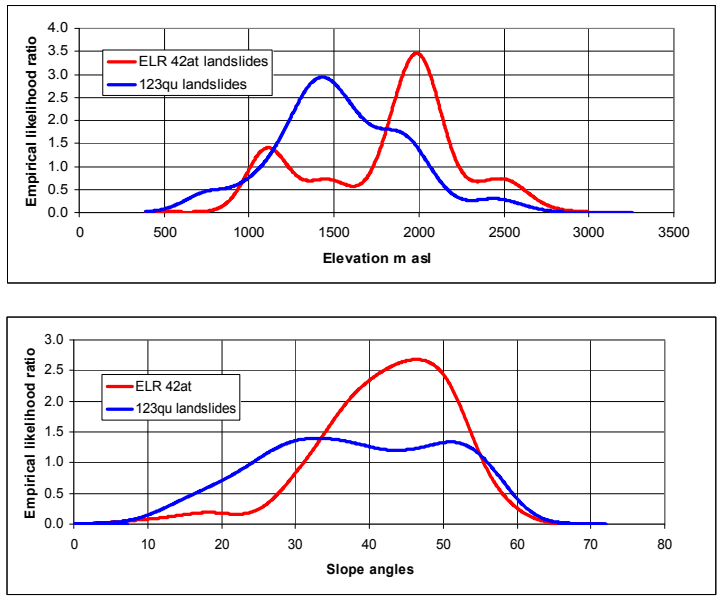

Figure 5: Empirical Likelihood Ratio functions for the elevation data layer and the slope data layer for the separate groups of 42 active landslide and 123 quiescent landslides trigger zones.

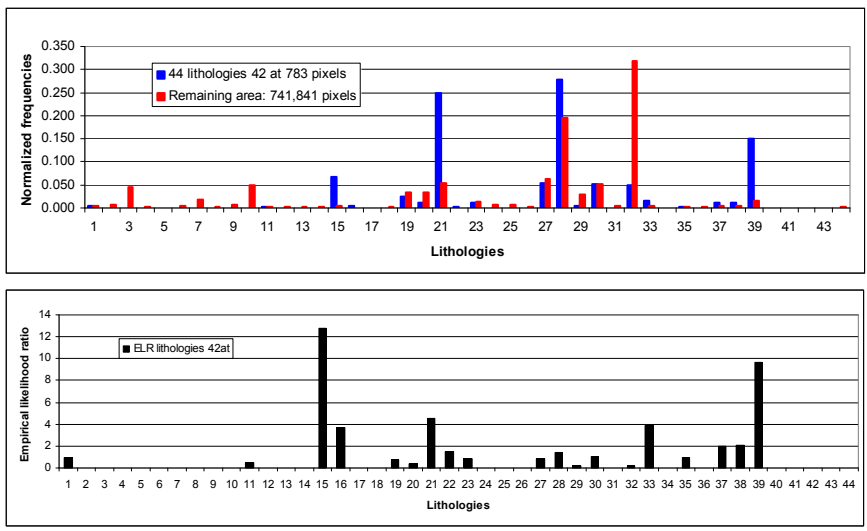

Figure 6: Normalized frequencies and Empirical Likelihood Ratios for the lithology data layer for the 44 active landslide trigger zones.

have high ELR values for units of accumulations from ancient rock falls and landslides (units 1, 2), poorly colonized alluvium fans and debris accumulations (units 8, 14), active and inactive partly colonized debris accumulations (22, 23), paleo-slides (33) and exposed effusive rocks (unit 35). Permeability classes of incoherent terrains and land use classes of areas covered by recent deforestation and with mixed and broad leaved coniferous plants show marginally significant ELR values for active landslides. Reforested and re-vegetated units have moderately significant ELR values for quiescent landslides.

The initial analysis of prediction modelling using the ELR shows clearly what units or values of ISPs contribute to the hazard prediction pattern generation. Our question to be answered, however, concerns how good the prediction patterns generated are as predictors of future landslides. For discovering that, we need to apply a number of cross-validations via blind-tests.

4 Processing strategies based on blind-tests

4.1 Motivation

Knowledge of the time or period of occurrence of the landslides is implied in assumption (3) in the previous section. The time can be obtained, for instance, by photo-interpreting aerial photographs covering a study area in different years. In that case the occurrences of an older period are used to generate a hazard prediction pattern, whose quality can be cross-validated by considering the distribution of later occurrences across the higher classes of the hazard prediction pattern. In most situations to date, however, the time or period of the occurrence of the landslides is unavailable. Then, in order to cross-validate the prediction pattern generated by using all the available occurrences (the most representative but whose predictive quality is still unknown, as is for the prediction patterns in Figure 2) we can simulate a time partition in various ways. For instance, when we have a few dozens of occurrences, we can pretend not to know the existence of one at a time, and use the remaining ones to generate a hazard prediction pattern. Subsequently, the cross-validation would consist of calculating which hazard class contains the excluded one. If we have, for instance, n occurrences, the process can be repeated n times with n-1 occurrences to obtain n classifications of occurrences.

Alternatively, we could select at random a part of the n occurrences, say 75%, use their distribution to obtain a hazard prediction pattern and see where the remaining 25% is classified in the hazard classes. Again, the process can be repeated as many times as needed to robustly cross-validate the initial hazard prediction pattern, whose relative prediction ability or "goodness" would have to be at least the same as, if not better than, that, of the cross-validated pattern.

Such ability can be visualized in the form of a prediction-rate table or histogram or cumulative plot. In addition, the statistics from such an iterative cross-validation process can produce what we can term as a *Target Pattern*, as an average or a median of all predicted values for each pixel, and an associated *Uncertainty Pattern*, expressing the variance of values or alternatively their

range at each pixel around the average values of the *Target Pattern*. Finally, some threshold of the classes in the *Target Pattern* will show all the pixels where the variance is below it, as a *Combination pattern* of target and uncertainty of class membership for the *Target Pattern*.

4.2 Application of sequential elimination of one and random selection strategies

Other types of strategies can also be applied, depending on the database characteristics and on the scope of the analysis. Here, the main focus is on database characterization and interpretation for generating hazard prediction patterns. In particular, our hazard priority in the Tirano North study area is the setting of the 42 active landslides, assumed to be more hazardous than the quiescent. Because their relationships with the other 123 quiescent landslides is rather weak, our analytical strategy has preferentially dealt with the setting of the former first and of the latter only later on as a term of comparison.

Figure 7 shows the *Target Pattern* obtained by calculating the median of the results of 42 ELR model prediction patterns obtained using each time the distribution of 42-1 active landslides to predict the remaining one. The corresponding prediction-rate curves are shown in Figure 8A. Ranking statistics has been used to obtain the median rank for the *Target Pattern* and the range of ranks as the *Uncertainty Pattern*. The 25% and 50% of the study area's *Target Pattern* have generated the *Combination Patterns*. Consider 42 prediction patterns. At every pixel, we have 42 prediction values. From these 42 values, we have computed the median and the range at each pixel. The *Target Pattern* in Figure 7 represents the median values and the *Uncertainty Pattern* represents the ranges. The higher is the value in the *Target Pattern*, the higher is the hazard. On the other hand, the higher is the value in the *Uncertainty Pattern*, the higher is the uncertainty. By selecting the areas whose pixels correspond to values that are included in the lowest 25% or 50% of the values in the *Uncertainty Pattern*, we are selecting the most stable (or robust) parts of the *Prediction Pattern* obtained from the 42 prediction patterns. To combine these two patterns into a *Combination Pattern*, we have shown the *Target Pattern* only in the selected 25% and 50% areas and we have coloured the remaining 75% or 50%areas as grey suggesting that there we have difficulty in predicting the level of hazard.

The prediction-rate curve sets in Figures 8A, 8B, and 8C, have been obtained by the ELR model in the following three analyses: (**42at-1x42**), 42 iterations of a sequential-elimination-of-one analysis of the active landslides, (**42at-r31x16**), 16 iterations of random selection of 31 of 42 of the active landslides to predict the remaining 11, and (**123qu-r92x16**), 16 iterations of random selection of 92 of the quiescent landslides to predict the remaining 31. In Figure 8A each thin line indicates the hazard class membership of one active landslide trigger zone. The solid line is the median prediction-rate curve as in the diagrams of Figures 8B and 8C, where the thin lines are the individual iteration prediction-rate curves.

We can see that the range of values around the median curve in the diagrams increases with the increase of cumulative proportion of study area classified as

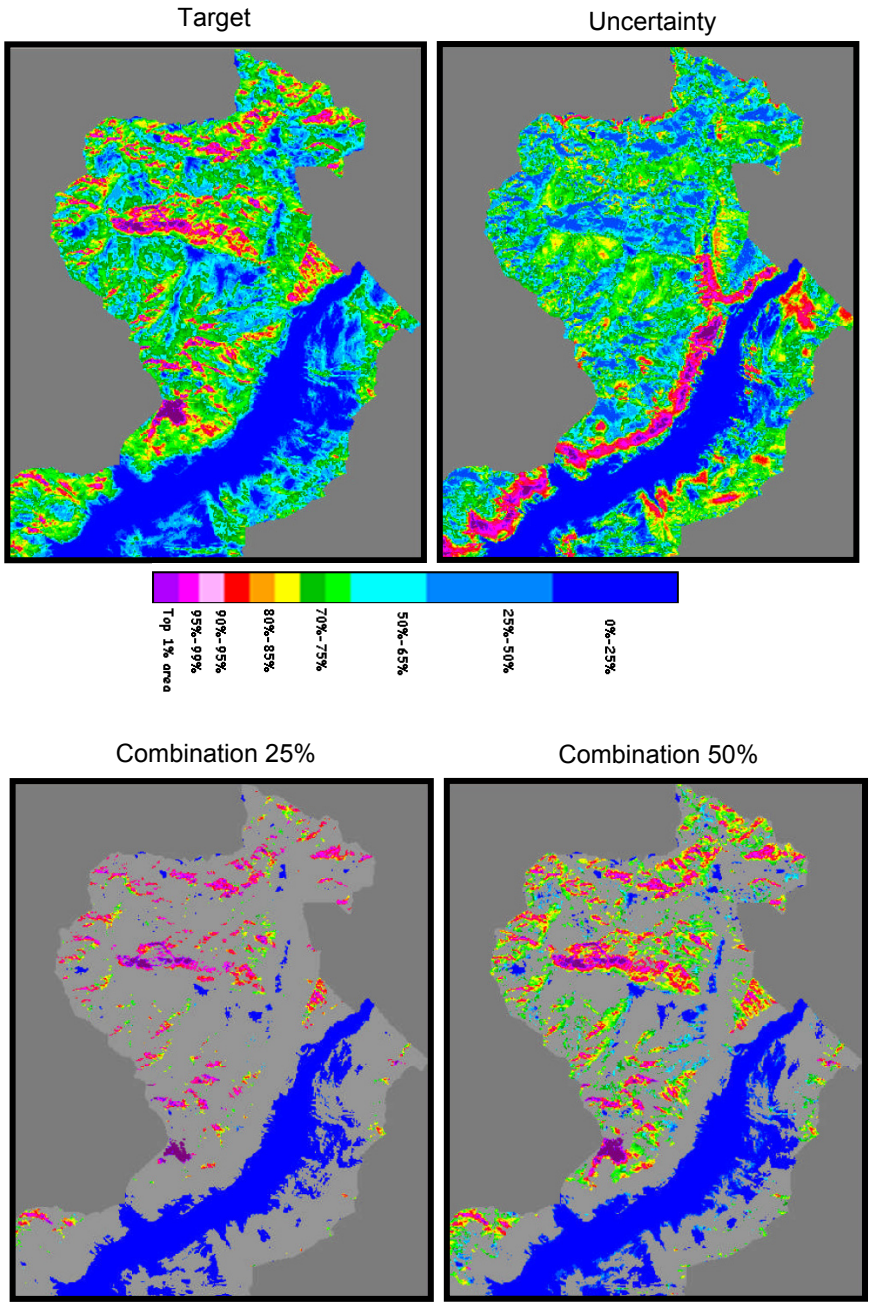

Figure 7: *Target*, *Uncertainty, 25%* and 50% *Combination Patterns* for analysis **42at-1x42**, using rank statistics, median rank and range of ranks.

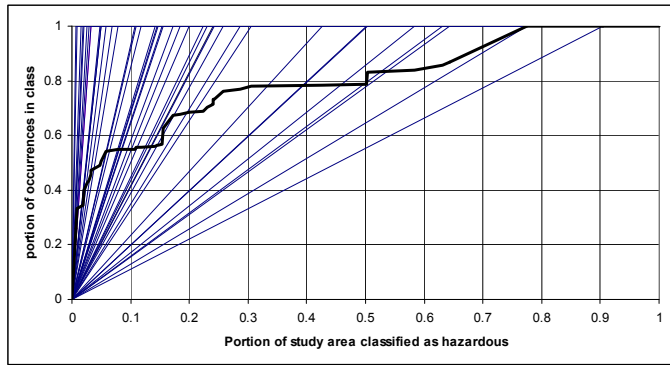

A

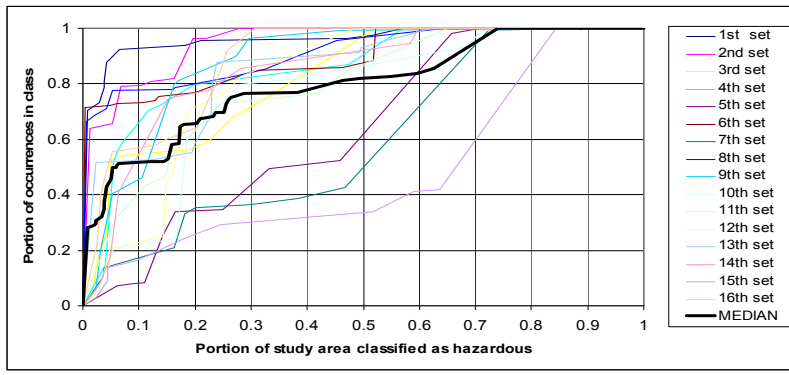

B

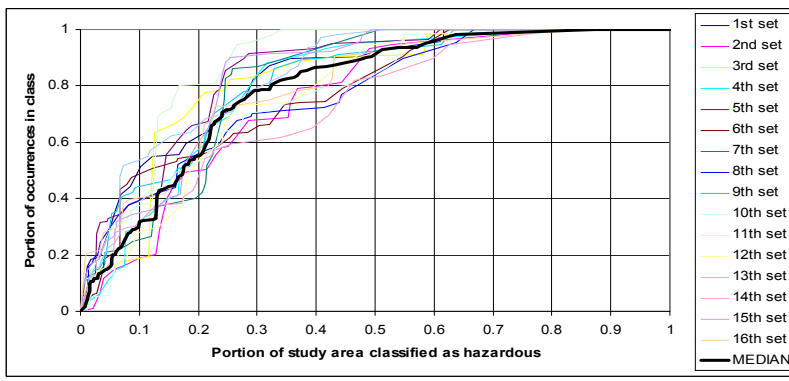

C

Figure 8: Sets of prediction-rate curves for the three analyses **42at-1x42** in (A), **42at-r31x16** in (B), and **123qu-r92x16** in (C). Solid curves are medians.

hazardous, to decrease towards the highest values on the horizontal axis. The median prediction-rate curve is initially very steep and then it tends to become less inclined until it gets sub-parallel to a diagonal line. A diagonal line indicates a random distribution of landslides in the hazard classes, i.e., a distribution directly proportional to the hazardous area increase. Intuitively, we can select the steeper part of the curve as indicative of the portion of study area to consider as hazardous within an acceptably narrow range of variance or uncertainty. Let us consider two points on the curves, at a 10% and a 20% of study area with the highest predicted value classes. What is the prediction telling us (or is able to tell us) that is acceptable from a benefit-cost point of view? The diagram in Figure 8A shows that 55% and 68% of the validation landslides fall within those respective classes. In the diagram of Figure 8B we have the 52% and 66%, just a little less than in the previous diagram, and in that of Figure 8C, we have 32% and 57%. In addition, the ranges of the predicted values are wider in Figures 8A and 8B, which show greater relative uncertainty than in Figure 8C.

4.3 Additional strategies: sequential selection of one and two regions

To analyze this aspect, another experiment was performed to verify the uniformity of the 42 active landslides and their setting. Each single active landslide trigger zone was used to generate a hazard prediction pattern to predict the remaining 41. It was repeated 42 times to obtain a 42x42 matrix of values, 41 for each landslide as a predictor and 41 as predicted by the remaining 41. A threshold on the classification was set arbitrarily at the highest 20% prediction classes. That enabled to isolate the 20 landslides considered simultaneously as well predicted and well predicting from the remaining 22. That clear cut separation indicated that also within the 42 active landslides there are at least two different settings. This should be of guidance in further improving their description in the landslide databases. A logical question to ask at this point is: can we improve further the prediction quality? Can we get better-looking steeper prediction-rate curves? The following analysis was to partly answer that question.

Another experiment was done assuming then to have at least two different settings of the 42 active landslides distributed randomly in the study area. We have tested the subdivision of the study area into two more or less geo-morphologically comparable E and W regions. The boundary of the two regions is indicated in Figure 1. The entire database was split into two sets of DSPs and ISPs. The 25 active landslide trigger zones in the E region were used to generate a prediction for the 17 active landslides in the W region and vice-versa. This was done by computing the spatial relationships within one region and exporting the respective statistics into the other. The results have generated more optimistic, better looking, prediction rates for the E to W prediction, with the highest 10% of the area classified as hazardous containing 72% of the validation landslides, and 20% containing 85%. For the W to E predictions the corresponding figures are for the 10% containing 46% and 20% containing 51%. While such E-W differences are due to the different distribution of units of ISPs in the two regions, the experiments indicate that a random mixture of landslide

types predicts relatively better another random mixture. It remains to be seen whether such better-looking prediction-rate curves are more useful for hazard mapping! The need for better characterization of the dynamic types of landslides and their setting remains a primary issue in prediction modelling.

5 Concluding remarks

In this contribution we have analyzed the spatial database constructed for the Tirano North study area. The purpose of the analyses was the assessment of its suitability for prediction modelling of rotational-translational landslide hazard. The 165 such landslide trigger zones mapped and described were partitioned into 42 active and 123 quiescent landslides. Their respective empirical likelihood ratios indicated different settings for the two classes of activity. The prediction pattern generated using the 123 quiescent landslides poorly predicts the 42 active landslides. Equally poor was the prediction pattern generated by the 42 active landslides for predicting the 123 quiescent landslides. Their different settings could be clearly interpreted in the analyses of the database from the empirical likelihood ratio functions of the eight data layers used as ISPs.

To assess the prediction capabilities of the two prediction patterns based on the 42 active or the 123 quiescent landslide trigger zones, several strategies were used for cross-validating via blind testing: (1) sequential elimination of one procedure for active landslides, named **42at-1x42**, (2) random selection for active landslides, named **42at-r31x16**, and (3) random selection for quiescent landslides, named **123qu-r92x16**. The iterative procedures generated sets of 42, 16 and 16 prediction patterns, respectively. Those sets were used to compute rank statistics generating the *Target Pattern* (median rank), the *Uncertainty Pattern* (range of ranks) and the *Combination Pattern* of Target and Uncertainty for given thresholds of uncertainty, i.e., 25%. Those patterns and the accompanying sets of prediction-rate curves indicate or measure the actual suitability of the database for spatial prediction modelling.

The relatively moderate prediction quality in the study area can perhaps be improved with a better characterization of the landslides identifying further their specific dynamic type and spatial setting. For instance, an analysis of the 42 active landslides was performed in which the spatial relationships of each individual landslide trigger zone were used to generate a prediction pattern and to cross-validate it with the distribution of the remaining 41. Forty two prediction patterns were generated iteratively and each provided a prediction rate curve for the remaining 41 landslides. This experiment allowed the separation of 20 well predicting and well predicted landslides from the remaining 22, poorly predicted and predicting (threshold at the highest 20% predicted classes). Finally, the E-W predictions generated better looking prediction-rate curves. Unfortunately, however, we had to use a mixture of different active landslides to predict another mixture. These aspects point at the insufficiency of the available description of the latter group of landslides. Only knowing more on the landslide settings and type we would obtain better results as more acceptable or interpretable hazard prediction patterns. It is not the model the main priority in

spatial prediction modelling, in this case, but the database quality for this purpose!

Acknowledgements

This contribution was partly supported by the European Commission's Project "Mountain Risks: from prediction to management and governance" (MRTN-CT-2006-035978, 2007-2010) [13]. SpatialModels Inc., Ottawa, Canada, has kindly provided a beta version of its new Spatial Target Mapping System, STM, [8].

References

[1] Chung, C.F. and Fabbri, A.G., Probabilistic prediction models for landslide hazard mapping. Photogrammetric Engineering and Remote Sensing PE and RS. **65(12)**, pp. 1389-1399, 1999.

[2] Fabbri, A. G. and Chung C.-J., On blind tests and spatial prediction models. *Natural Resources Research*, **17(2)**, pp. 107-118, 2008.

[3] Mauriello M. R., Previsione di Pericolo di Frana nell'Area di Tirano Nord: Incertezza di Valori di Favorabilità (Prediction of landslide hazard in the Tirano North Area: Uncertainty of Favorability Values). Unpublished M. Sc. Thesis, University of Milano-Bicocca, Milan, Italy, 146 p., 2008.

[4] APAT, Field Trip Guide Book, P05. Volume n° 3, 32nd International Geological Congress: Italian Alpine Landslides- Guerrieri L., Rodia I., Serva L. – Published by APAT, Rome, 2004.

[5] IFFI http://www.isprambiente.gov.it/site/it-IT/Progetti/www.sinanet.apat.it/progettoiffi.

[6] CARG http://www.isprambiente.gov.it/site/it-IT/Progetti/Progetto_CARG_-_Cartografia_geologica_e_geotematica/www.cartografia.regione.lombardia.it /CARGWEB/www.gitonline.eu/pdf_sanleo/orali/Brunori.pdf.

[7] DUSAF http://www.ersaf.lombardia.it/servizi/Menu/dinamica.aspx?idArea=16914&idCat=17254&ID=17254http://www.territorio.regione.lombardia.it/cs/Satellite?c=Page&childpagename=DG_Territorio%2FDGLayout&cid=1213441282211&p=1213441282211&pagename=DG_TERRWrapper www.tedoc.polimi.it/download/DUSAF.pdf http://www.cartografia.regione.lombardia.it/geoportale Search: DUSAF.

[8] www.spatialmodels.com

[9] Fabbri A.G. and Chung C.-J., Training decision-makers in hazard spatial prediction and risk assessment: ideas, tools, strategies and challenges. *Disaster Management and Human Health Risk,* eds. K. Duncan and C. A. Brebbia, Southampton, WIT Press, p. 285-296, or WIT Transactions on the Built Environment, www.witpress.com, ISSN 1743-3509 (on-line) doi:10_2495/DMAN09025, 2009.

[10] Fabbri, A.G. and Chung C.-J., A spatial prediction modeling system for mineral potential and natural hazard mapping. Proceedings of EUREGEO2012, Bologna, Italy, June 12-15, 2 p., in press, 2012.

[11] Fabbri, A.G., Chung, C.-J. and D.-H. Jang, A software approach to spatial predictions of natural hazards and consequent risks. *Risk Analysis IV,* ed. C.A. Brebbia, Southampton, Boston, WIT Press, p. 289-305, 2004.
[12] Chung, C.-J., Using likelihood ratio functions for modelling the conditional probability of occurrence of future landslide for risk assessment. *Computers and Geosciences*. **32**, pp. 1052-1065, 2006.
[13] http://www.unicaen.fr/mountainrisks/spip/spip.php?page=index